Features of the Auger resonant Raman effect in experimental spectra

E. Kukk, S. Aksela, and H. Aksela
Department of Physical Sciences, Oulu University, FIN 90570 Oulu, Finland
(Received 27 November 1995)

The influence of the photon bandwidth on the line shapes of the resonant Auger electron spectra has been studied. The observed features have been explained as due to the Auger resonant Raman effect, which has been extended to cover the cases of nonmonochromatic excitation. Changes in the line shapes and also several specific effects, connected with detuned excitation, have been demonstrated by experimental examples, matched with model calculations. The lifetime interference phenomenon, appearing in the decay of several close-lying resonance states to the same final state, is regarded together with the influence of the limited photon bandwidth. Special attention is paid to the problems of data handling. [S1050-2947(96)02505-3]

PACS number(s): 32.80.Hd, 32.70.Jz

I. INTRODUCTION

The Auger resonant Raman effect and some of its consequences have become well known through recent theoretical and experimental studies [1–11]. The Auger resonant Raman effect (ARRE) was first observed in the x-ray energy range [1], but recently also in the vacuum ultraviolet (vuv) range [3,4] thanks to rapid improvements in the experimental photon and electron energy resolutions. The most outstanding consequence of ARRE is that if a resonance state is excited by a very narrow photon band, then the linewidths in the Auger electron spectrum can be much narrower than the lifetime width of the core-excited resonance state. This has made possible a great improvement in high-resolution resonant Auger spectroscopy, with very promising future prospects. Excitation with nearly monochromatic radiation also allows one to observe a linear disperion of the kinetic energy of the resonant Auger electron line with photon energy, which is usually taken as a fingerprint of ARRE [1,3,4].

In this paper the term ARRE is extended to cover a broad variety of effects, observable in the electron spectra, when the monochromaticity of the excitation is not stringent, but the photon bandwidth is comparable with the lifetime width. ARRE affects line energies, intensities, and line shapes in the resonant Auger spectra in a quite specific way in such cases. It can even lead to astonishing results such as double-peak structures, as demonstrated in our previous study [11]. The aim of this paper is to give an overview of the typical ARRE features that appear in the resonant Auger spectra under usual conditions of a high-resolution experiment in the vuv photon energy range. A number of spectra were recorded under various experimental conditions, thus allowing one to specify the regions where the observed effects are most pronounced. The experimental data are compared with the calculations, based on a statistical model given by Armen and Wang [10], with the parameters adjusted to represent the given experimental conditions.

A krypton resonant Auger spectrum was chosen as a test object and the spectra were recorded, systematically varying the energy and width of the exciting photon band. The analysis of these spectra provides the first experimental demonstration of several ARRE features predicted by the model calculations [10]. The provided examples should help to discover analogous features in other spectra. Also, the practical formulas for resonant Auger line shapes and intensities are provided as a starting point for proper data handling of the spectra influenced by ARRE. Special attention is paid to the hazards connected with the use of the traditional data handling methods. The ARRE features are also compared with the effect of lifetime interference arising if the Auger transitions from several close-lying resonance states reach the same final state [12–14]. These two effects can often occur together and manifest themselves in a rather similar way in the electron spectra.

II. EXPERIMENT

The spectra have been measured at the Finnish beamline (BL 51) at the MAX-I storage ring in Lund, Sweden [15,16]. Synchrotron radiation in the photon energy range 60–600 eV, obtained from a short-period undulator, is monochromatized by a modified SX-700 plane grating monochromator [17]. The beamline is equipped with a differential pumping section that reduces the pressure by five orders of magnitude between the experimental station and the monochromator. The spectra were recorded with a hemispherical sector electron analyzer [18], mounted in the pseudomagic angle relative to the electric vector of the photon beam. Electrons were retarded to constant pass energy of 10 eV by using a lens system before the analyzer, which gave electron energy resolution less than 50 meV. The electron spectra were recorded using different monochromator's exit slit widths, thus varying the width of the photon band.

III. THEORY

The theoretical basis of ARRE, as observed in electron spectra, is the radiationless resonant Raman scattering (RRS) theory, which has been developed in a number of extensive studies (see Refs. [8,9] and references therein). In the following, we shall restate briefly the main results of the radiationless RRS theory for the case of nonmonochromatic excitation in a statistical form [10], directly applicable in the analysis of provided experimental examples. The given model is restricted to only one involved resonance state and also neglects direct scattering amplitudes.

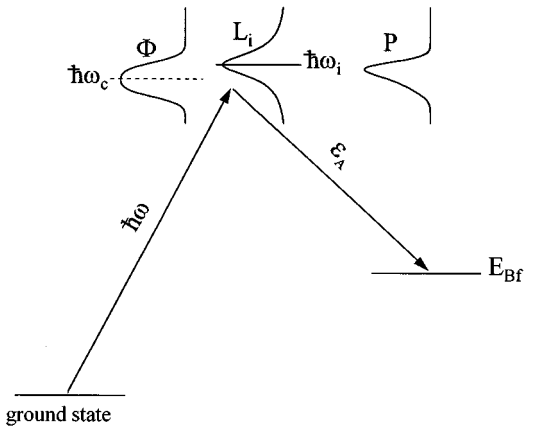

FIG. 1. Schematic representation of the photoexcitation and Auger decay processes, with photon band (Φ), lifetime broadening (L_i), and Auger electron distribution (P) shown.

The radiationless RRS theory handles the resonant photoexcitation and the Auger decay as a single scattering event from an initial state, consisting of an incoming photon and the atom in its ground state, to a final state — an ejected Auger electron and singly ionized atom. The core-excited intermediate resonance state acts, from a statistical point of view, as a bandpass filter selecting the photons with suitable energy to participate in the scattering process. Such filtering selects the photons with energy $\hbar\omega$ around the nominal resonance energy $\hbar\omega_i$, in the range limited by the Lorentzian lifetime broadening of the resonance state, $L_i(\hbar\omega-\hbar\omega_i,\Gamma_i)$ with a width Γ_i (see Fig. 1). Absorption of a photon $\hbar\omega$ yields an Auger electron with kinetic energy

$$\epsilon_A=\hbar\omega-E_{Bf}, \tag{1}$$

where E_{Bf} is the binding energy of the singly ionized atomic final state. The probability for absorbing a photon $\hbar\omega$ and ejecting an electron with energy ϵ_A is determined by the Lorentzian distribution $L_i(\hbar\omega-\hbar\omega_i,\Gamma_i)$. It is, naturally, highest at the nominal resonance energy $\hbar\omega_i$, at which an Auger electon with nominal energy ϵ_{A0} is ejected. It is assumed throughout this paper that the final state is stable against further decay and has negligible width. This is a common case for the vuv-range excitations, where the final-state vacancies are usually created in the valence orbitals.

In practice, the exciting radiation is not monochromatic, but the photons form a band with energy distribution $\Phi(\hbar\omega-\hbar\omega_c,\Gamma_p)$, centered at $\hbar\omega_c$ and having width Γ_p. The Auger electron energy distribution is given by

$$P(\epsilon_A)\propto\Phi(\hbar\omega-\hbar\omega_c,\Gamma_p)L_i(\hbar\omega-\hbar\omega_i,\Gamma_i). \tag{2}$$

The further analysis of ARRE features in vuv-range resonant Auger spectra is based on Eq. (2). (Hard x rays can excite deep core orbitals and then an additional convolution with the lifetime broadening of the unstable final state must be performed in order to obtain the Auger electron energy distribution.)

It is worthwhile to point out some apparent consequences of Eq. (2) before proceeding to the experimental examples. The right-hand side of Eq. (2) is a simple product of two distribution functions and consequently, if their widths are very different, then the distribution $P(\epsilon_A)$ is governed by the narrower one. This useful property means, for example, that the excitation with a very narrow photon band eliminates the lifetime broadening from the observed resonance Auger spectrum. On the other hand, if the photon band is so broad that it can be taken as a constant over the lifetime width, then $P(\epsilon_A)$ has the Lorentzian shape $L_i(\hbar\omega-\hbar\omega_i,\Gamma_i)$. Many experimantal situations fall in between these extrema and then the analysis of the spectra is more complicated.

It is essential to notice that the distribution $P(\epsilon_A)$ is centered at the nominal resonance Auger electron energy ϵ_{A0} only if $\hbar\omega_c$ equals $\hbar\omega_i$, that is, if the exciting photon band is tuned exactly to the resonance. If the excitation is detuned from the resonance, then the maximum of the electron energy distribution is shifted away from ϵ_{A0}. The shift is a function of the photon energy detuning, defined as

$$\Delta=\hbar\omega_c-\hbar\omega_i. \tag{3}$$

Again the two extreme cases can be stated. Under the excitation with a very broad photon band $P(\epsilon_A)$ shows no dispersive behavior against the detuning Δ, whereas the monochromatic excitation results in a strictly linear dispersion of ϵ_A against Δ,

$$\epsilon_A=\epsilon_{A0}+\Delta. \tag{4}$$

The total probability for exciting a resonance state and emitting an Auger electron can be obtained as

$$I(\Delta)=\int_0^\infty P(\epsilon_A)d\epsilon_A, \tag{5}$$

or, using Eq. (2),

$$I(\Delta)\propto\int_0^\infty\Phi(\hbar\omega-\hbar\omega_c,\Gamma_p)L_i(\hbar\omega-\hbar\omega_i,\Gamma_i)d\omega. \tag{6}$$

The total probability $I(\Delta)$ (which is related to the line intensity in the spectrum) is a function of photon energy detuning and has a profile governed by broader distribution in Eq. (6).

The observed resonant Auger line shapes are not given directly by $P(\epsilon_A)$, but are broadened by the spectrometer function $G(\epsilon,\Gamma_g)$ of the electron spectrometer. The observed line shapes are the convolutions

$$P_{\rm obs}(\epsilon)=\int_0^\infty G(\epsilon-\epsilon_A,\Gamma_g)P(\epsilon_A)d\epsilon_A. \tag{7}$$

The convolution complicates the observation of the ARRE features by changing the line shapes and shifting peak maxima of asymmetric lines.

IV. PHOTON BANDS

It is of crucial importance to find out the distribution function $\Phi(\hbar\omega-\hbar\omega_c,\Gamma_p)$ for the exciting photon band before starting the analysis of the observed ARRE features. The photon band can be determined from separate measurements or from the electron spectrum to be analyzed. The photoelectron lines from the direct ionization of the valence orbitals are also present in the electron spectra, often close to the

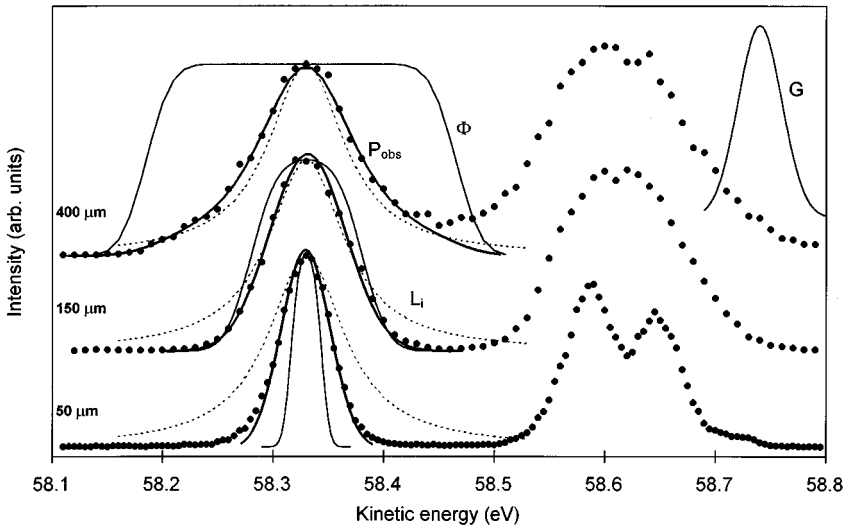

FIG. 2. Part of the Kr $3d_{5/2}^{-1}5p \rightarrow 4p^{-2}5p$ resonant Auger spectrum, excited using various exit slit widths of the monochromator. For details see text.

Auger electron lines. The photoelectron line shape in the spectrum is given by the photon band $\Phi(\hbar\omega-\hbar\omega_c,\Gamma_p)$, convoluted with the spectrometer function $G(\epsilon,\Gamma_g)$. Our spectrometer function (shown in Fig. 2) has the full width at half maximum (FWHM) $\Gamma_g=46$ meV and has been taken as a Gaussian profile. If the photon bandwidth Γ_p is not much smaller than Γ_g, then a reliable estimate for $\Phi(\hbar\omega-\hbar\omega_c,\Gamma_p)$ can be obtained by deconvoluting the photoelectron line with the spectrometer function.

A plane grating monochromator with only one, the exit slit, was used in our experiment. In such a monochromator design the photon band is formed as a convolution of the exit slit contribution to the total width (a rectangular function) with several other contributions, which can be approximated by a single Gaussian function. The spectrometer function is also supposed to be a Gaussian, so that the photoelectron line can be fitted with a convolution of rectangular and Gaussian functions. The photon bands were obtained by deconvoluting such fit curves with the spectrometer function. The results for the monochromator's exit slit widths of 150 and 400 μm can be seen in Fig. 2. The photon band determined with the exit slit width of 50 μm is considerably narrower than the spectrometer function and the described deconvolution procedure is rather unreliable. Thus an independent estimate for $\Phi(\hbar\omega-\hbar\omega_c,\Gamma_p)$ has been used in this case (also shown in Fig. 2).

The FWHM's of the photon bands in Fig. 2 are 26, 100, and 280 meV for 50-, 150-, and 400-μm exit slit widths, respectively. In comparison of these bandwidths with the lifetime broadening of the resonant state, $\Gamma_i=83$ meV, one can see that the cases $\Gamma_p<\Gamma_i$, $\Gamma_p\simeq\Gamma_i$, and $\Gamma_p>\Gamma_i$ are covered, allowing one to trace the ARRE features in these three different regions.

The photon bands of our SX-700 monochromator are accompanied by a weak tail at low-energy side [11], which is a very specific feature and is therefore, for the sake of generality, not included in our simulations. The neglect of this tail may cause some discrepancies between the experiment and calculations.

V. LINE NARROWING AND TAIL CUTOFF IN THE AUGER ELECTRON SPECTRA

Figure 2 presents three Kr $3d_{5/2}^{-1}5p \rightarrow 4p^{-2}5p$ resonant Auger spectra, excited with photon bands of different width. The exciting photon bands, as well as the lifetime broadening and the spectrometer function, are also shown in Fig. 2. The photon band was tuned exactly to the nominal resonance energy ($\hbar\omega_c=\hbar\omega_i$, $\Delta=0$) in all cases. The kinetic energy range of Fig. 2 covers the transitions $3d_{5/2}^{-1}5p \rightarrow 4p^{-2}(^1D)5p(^2D_{3/2,5/2},^2P_{1/2})$ at 58.32 eV and $3d_{5/2}^{-1}5p \rightarrow 4p^{-2}(^1D)5p(^2F_{5/2,7/2},^2P_{3/2})$ around 58.6 eV. Calculations [19] indicate that the peak at 58.32 eV is composed mainly of the transitions to the $4p^{-2}(^1D)5p(^2D_{3/2,5/2})$ states, which lie very close in energy (separated by 15 meV), whereas the transitions to the $4p^{-2}(^1D)5p(^2P_{1/2})$ state are much less intense. This peak is therefore the most suitable, although not ideal, for studying the ARRE line-shape features.

The uppermost spectrum in Fig. 2 is excited by a photon band having a width much larger than the lifetime width of the resonant state. The Auger line shape is now determined almost solely by $L_i(\hbar\omega-\hbar\omega_i,\Gamma_i)$ in Eq. (2), which must be convoluted by the spectrometer function $G(\epsilon,\Gamma_g)$ to fit the experimental data points. The line shape is well described by a Voigt profile and only a weak discrepancy far at the Lorentzian tail at the low kinetic energy side indicates the influence of the limited width of the photon band.

The middle spectrum has been recorded with a photon band of a width nearly equal to the lifetime width. In this case no approximations can be made and the Auger electron energy distribution is properly given only by Eq. (2) [and the observed line shape by Eq. (7)]. The line shape is rather broad at the peak maximum, but decreases rapidly at the tails, so that the line actually resembles a Gaussian profile. Such a ''tail cutoff'' of the Lorentzian is typical for ARRE in the photon bandwidth range $\Gamma_p\simeq\Gamma_i$ and is due to the multiplication of the two distribution functions in Eq. (2). The effect is especially pronounced in our spectrum, because the photon band has relatively sharp edges, but is, on the other hand, somewhat veiled by the instrumental broadening of the spectrometer.

The lowest spectrum in Fig. 2 has been excited by the narrowest photon band, which practically determines the Auger electron distribution in Eq. (2), so that the observed line shapes can be approximated by a convolution of the photon band with $G(\epsilon,\Gamma_g)$. In this spectrum, the Auger line is

clearly narrower than the lifetime broadening, even after being broadened by the spectrometer function. This is the ARRE feature with the greatest practical importance, as it allows one to improve the electron energy resolution and separate very fine details and energy splittings in the resonant Auger spectra. Some deviations of the calculated curve from the measured spectrum are probably due to the fact that the real shape of the spectrometer function differs somewhat from the Gaussian profile.

The physically correct line shapes for the Auger spectra in Fig. 2 are provided by Eqs. (1) and (7). In many cases, however, some analytical functions with several adjustable parameters (like Voigt or pseudo-Voigt profiles) may be flexible enough to give a good fit to the spectrum. The minor deviations that arise when using such profiles are not critical when studying single well-separated peaks, although some of the parameters, e.g., Gaussian and Lorentzian widths in the Voigt profile, have lost their physical meaning. But the use of such line profiles can lead to severe errors, if applied to studying heavily overlapping structures with largely varying peak intensities (such as the higher kinetic energy structure in Fig. 2).

VI. EFFECTS OF PHOTON ENERGY DETUNING

A. Auger line dispersion and line-shape distortions

The energies of the emitted Auger electrons shift in the kinetic energy scale when the photon band is detuned from the nominal resonance energy. The dispersion varies from linear [Eq. (4)] to constant, depending on the width of the photon band. In the following, the $3d_{5/2}^{-1}5p \rightarrow 4p^{-2}(^1D)5p(^2D_{3/2,5/2})$ lines in the Auger spectra, recorded with variable photon energy detuning Δ, are analyzed. Two series of spectra have been recorded, using different photon bandwidths [$\Gamma_p = 100$ meV (exit slit width 150 μm), see Fig. 3, and $\Gamma_p = 26$ meV (50 μm), see Fig. 4]. The photon bands were shown in Fig. 2. The peaks are normalized to the same intensity for better visualization in Figs. 3 and 4, although the actual differencies in the intensities are large (as discussed in Sec. VI B).

We prefer to use the Auger electron mean energy rather than the peak maximum position for the description the peak location, as it can be evaluated more accurately and its determination does not require any preliminary assumptions about the Auger line shape. Also, the convolution with the symmetrical spectrometer function does not alter the mean energy of a peak, even if it is asymmetrical, although the peak maximum shifts in such a case. The mean energies from model calculations using Eq. (2) are therefore directly comparable with the experimental data.

The photon energy detuning Δ can be roughly estimated from the monochromator's readings, but can be determined also using the kinetic energy of the photoelectron lines, which shift linearly with Δ. It has been assumed that the kinetic energy scale did not shift when recording one series of spectra, which could introduce a systematic error when determining Δ. The other factors affecting the accuracy of the values of Δ are the statistical error in determining the kinetic energies of the photolines and, most importantly, a systematic error from locating the resonance maximum $\hbar\omega_i$, as the reference from which the detuning is measured.

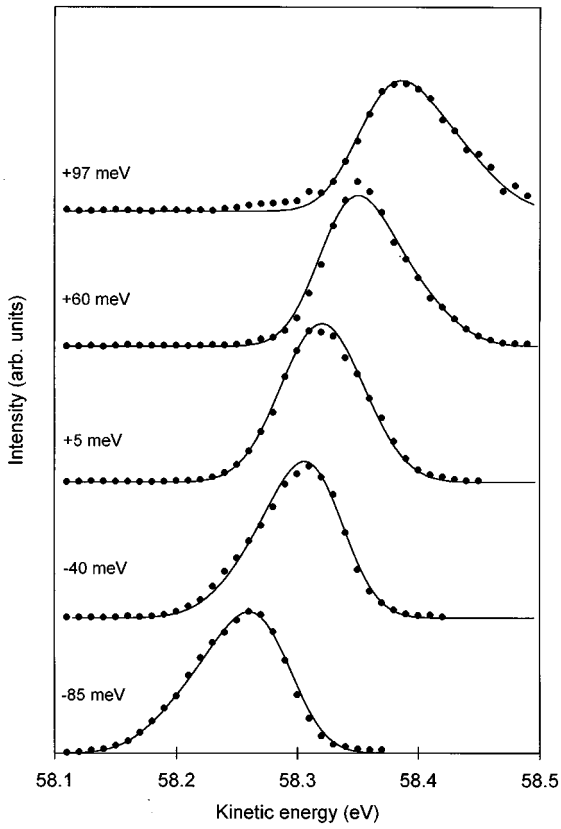

FIG. 3. Kr $3d_{5/2}^{-1}5p \rightarrow 4p^{-2}(^1D)5p(^2D_{3/2,5/2})$ lines in the Auger spectra, recorded with the photon band detuned from exact resonance (detuning shown for each spectrum). Monochromator's exit slit width set to 150 μm.

1. Photon bandwidth and lifetime width comparable

This is the situation for the spectra in Fig. 3, recorded with the 100-meV photon band (150 μm slit width). The photon energy detuning Δ is marked next to each spectrum. Figure 3 also shows the calculated line profiles at the given detuning values. To fit the experimental spectrum, the calculated electron energy distributions [Eq. (2)] have been convoluted with the spectrometer function [Eq. (7)]. Slight adjustments (± 5 meV) of the kinetic energies of calculated profiles was needed to obtain a better fit, due to the limited accuracy of the method for determining the photon energy detuning. Apart from obvious line shifts, asymmetrical line shapes can be observed. The asymmetry is the strongest at the detunings $\Delta \simeq \pm \Gamma_i$. The asymmetric tail appears at the high kinetic energy side if the photon band is tuned above the resonance and at the low kinetic energy side if it is tuned below the resonance. At smaller and larger detuning values the asymmetry disappears gradually. At very large detunings (not shown in Fig. 3) the Auger line profile approaches that of the photon band. The development of asymmetry in line shapes is reflected also in the linewidths, which are the smallest at exact tuning and largest for the most asymmetric profiles.

The asymmetry is easily observable in Fig. 3, but can be harder to detect in the spectra with complex structure, where it can strongly alter the apparent intensity ratios of close-lying peaks, if these are fitted by symmetric profiles. For example, in the structure around 58.6 eV in Fig. 2, a 50-meV

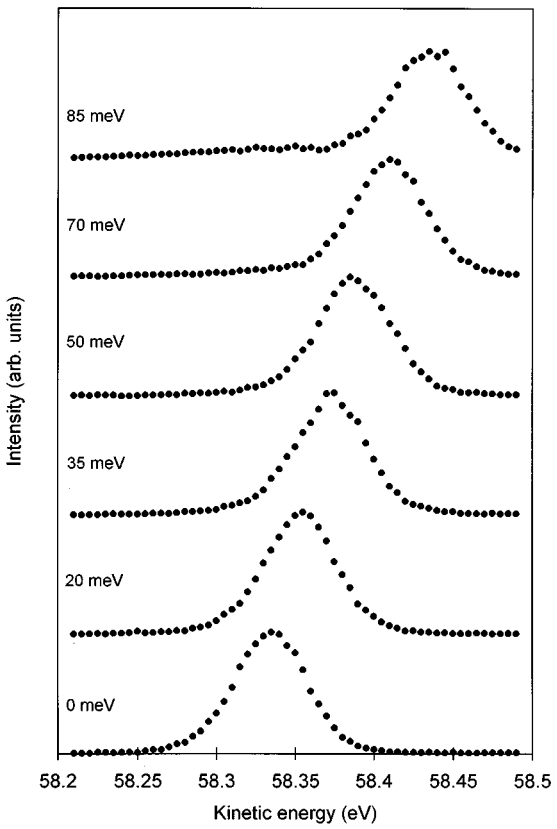

FIG. 4. Same as Fig. 3, but the exit slit width set to 50 μm.

photon energy detuning leads to errors up to 50% in the branching ratios of the main peaks if symmetric line shapes are used.

The mean energies of the Auger electrons, determined from the experiment, are shown in Fig. 5 as a function of Δ. The solid curve is provided by model calculations, using Eq. (2) and scanning the photon band (Γ_p=100 meV) across the Lorentzian lifetime distribution (Γ_i=83 meV). Figure 5 displays a clear deviation from linear dispersion, as predicted by Armen and Wang [10]. The deviation is the largest (about 20 meV) at the detuning $\Delta=\pm 80$ meV, coinciding with the region of the largest asymmetry.

2. Photon bandwidth smaller than the lifetime width

The spectra in Fig. 4, recorded using a narrow (Γ_g=26 meV) photon band, possess the same principal features as the spectra in Fig. 3. In this bandwidth region, however, these features become more subtle and hard to observe. For example, no difference from the linear dispersion of the mean energy of Auger electrons with the detuning can be observed. This result agrees well with calculations, which show that the largest deviation is less than ± 2 meV (as compared to ± 20 meV in the previous case), which is beyond the experimental accuracy. Thus, the approximation $\Gamma_p \ll \Gamma_i$, leading to Eq. (4), holds well, although Γ_p is only about three times smaller than Γ_i. The line shapes in Fig. 4 should also display slight asymmetries, in analogy with Fig. 3, but it is hardly observable, as the asymmetry is largely eliminated by the spectrometer broadening.

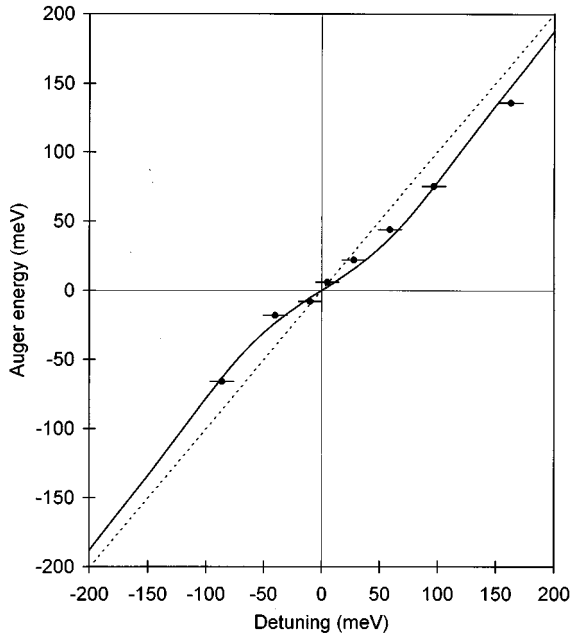

FIG. 5. Mean kinetic energy of the Kr $3d_{5/2}^{-1}5p \rightarrow 4p^{-2}(^1D)5p(^2D_{3/2,5/2})$ Auger electron line, plotted vs photon energy detuning. Experimental values (●) shown relative to the nominal energy ϵ_{A0}, together with a simulated curve. Straight line corresponds to linear dispersion.

3. Spectra from two close-lying resonance states

If the photon band is tuned in between two close-lying resonance states so that both are excited simultaneously, then the Auger electron spectrum consists of two different sets of line shapes, with opposite asymmetries and dispersive characteristics. Furthermore, if these two (or more) resonance states decay into the same final state, then the limited photon bandwidth is not the only cause of line shifts and line-shape distortions. One must also take into account the effect of lifetime interference, so that the electron energy distribution is

$$P(\epsilon_A) \propto \Phi(\hbar\omega-\hbar\omega_c,\Gamma_p)\left|\sum_i \frac{M_{i0}M_{fi}}{\hbar\omega-\hbar\omega_i+i\Gamma/2}\right|^2, \quad (8)$$

where M_{i0} and M_{fi} are the transition matrix elements for the photoexcitation and Auger decay, respectively. The square of the sum of the complex scattering amplitudes over the intermediate resonance states in Eq. (8) is not just a sum of two Lorentzian functions as would emerge using Eq. (2), but is modified by interference terms, which become important if the separation of the resonance states is of the order of their lifetime width. The lifetime interference is well known in molecular systems, arising from the transitions from adjacent vibrational levels, but can be found also in the atomic transitions from different electronic states (state interference in Ref. [13]). Here we present both effects, ARRE (as connected to limited photon bandwidth) and lifetime interference, together, but also show their individual contributions. Their separation is rather formal, as the nonradiative RRS theory, developed in its full extent, includes both effects. The

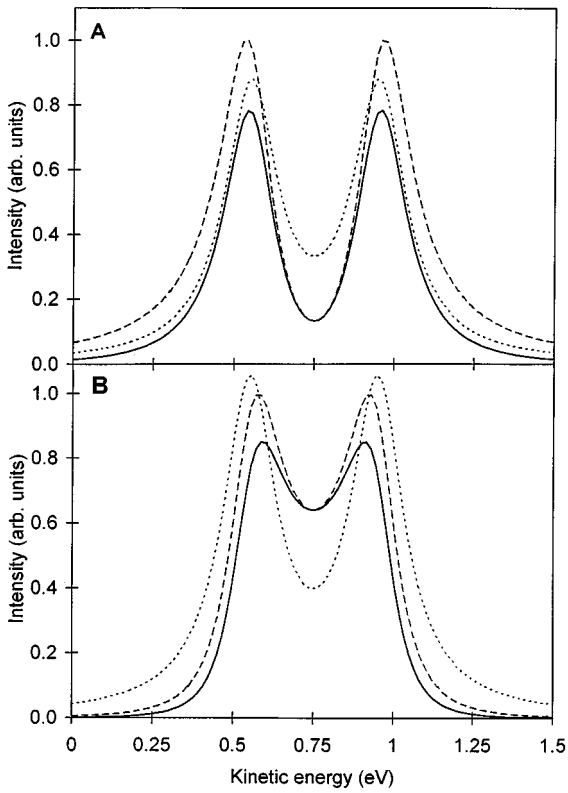

FIG. 6. Modeled spectrum of Auger decay from two adjacent resonance states to a single final state. (a) and (b) show the calculated results for 0° and 180° phase shifts, respectively. Dotted curves: interference excluded, constant photon band; dashed curves: interference included, constant photon band; solid curves: interference included, photon band taken as Gaussian with 800 meV FWHM.

parameters for the calculated spectra have been chosen arbitrarily, so that a good visualization of the studied effects is obtained.

Figure 6 shows a modeled Auger electron spectrum of the transitions from two adjacent resonance states with $\Gamma_i = 200$ meV, separated by 400 meV. The spectra are calculated using Eq. (8), with the numerators $M_{i0}M_{fi}$ in the sum taken as real and with equal absolute values. For panels (a) and (b) the numerators have the same and opposite sign (0° and 180° phase shift), respectively. The dotted curves have been calculated by excluding the interference terms in Eq. (8) and by taking Φ as constant, i.e., neglecting also the influence of limited photon bandwidth (ARRE). The dotted curves in Fig. 6 are superpositions of two Lorentzians, reflecting the resonance states. For the dashed curves, the interference terms were included, but ARRE was still neglected by taking $\Phi = \text{const}$. The comparison of panels (a) and (b) shows that the interference depends critically on the phase shift, removing intensity from the central area in panel (a), but gathering intensity to the center in panel (b).

The solid curves have been obtained by including interference terms in Eq. (8) and adding the influence of the limited photon band by taking Φ as a Gaussian with $\Gamma_p = 800$ meV, centered between the resonances. The comparison of the dashed and solid curves in panels (a) and (b) shows that ARRE always enhances the central region of the spectra.

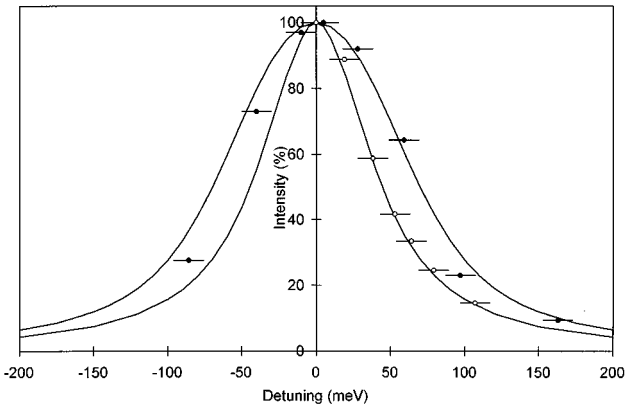

FIG. 7. Total intensity of Kr $3d_{5/2}^{-1}5p \rightarrow 4p^{-2}(^1D)5p(^2D_{3/2,5/2})$ Auger lines as a function of photon energy detuning. Experimental data at 50 μm (○) and 150 μm (●) monochromator exit slit widths are plotted together with the results of model calculations (solid lines).

Decreasing the photon bandwidth would shift the two peaks together and finally merge them into a single peak.

Thus, ARRE and the interference effect, although very similar in appearance, add up in spectrum (b), but nearly cancel each other in spectrum (a). In reality, the interplay between them is much more unpredictable, depending on many factors. The contribution from ARRE would increase rapidly when using narrower photon bands and the interference effect would dominate, if the resonance states were closer to each other. But both effects should be taken into account often when analyzing an experimental spectrum.

B. Intensity decrease

The most easily observable property of the spectra excited with the detuned photon band is the strongly reduced intensity of the resonant Auger electron lines. This can change the overall appearance of the electron spectrum, as the resonance Auger electron lines are usually overlapping with the lines from direct photoionization, whose intensity is unaffected by the photon energy detuning (see, e.g., Ref. [11]). The intensity of the Auger lines relative to the photoelectron lines therefore provides a means to determine the intensity decrease under the detuned excitation — the intensity ratio of the Auger versus photoelectron lines is largest at the exact resonance and decreases as a function of the detuning. The provided method for determining the intensity decrease of the Auger lines is applicable, if the participator Auger decay channel that enhances the photoelectron line intensities can be neglected.

The intensity of an Auger line in the measured spectrum is given by integrating over the Auger peak. Figure 7 shows the relative intensity of the $3d_{5/2}^{-1}5p \rightarrow 4p^2(^1D)5p(^2D_{3/2,5/2})$ Auger line as a function of detuning. The two sets of the data points correspond to the spectra, excited with the 100-meV-wide (filled dots) and 26-meV-wide (open dots) photon bands. The curves in Fig. 7 are provided by model calculations using Eq. (6). The curves are symmetrical with respect to the exact tuning, so far as the photon band distribution $\Phi(\hbar\omega - \hbar\omega_c, \Gamma_p)$ is symmetrical. The curves are convolutions of the photon band and lifetime

broadening and have the FWHM's of 140 meV (Γ_p=100 meV, Γ_i=83 meV) and 89 meV (Γ_p=26 meV, Γ_i=83 meV). The latter curve represents quite well the shape and width (Γ_i=83 meV) of the Lorentzian lifetime broadening of the resonant core-excited state. Thus, a reversed procedure — fitting the experimental intensities with a modeled curve obtained with a known photon band and varying the lifetime width — can be regarded as a method for determining the lifetime width (as proposed in Ref. [10]). Note that the spectrometer function does not broaden the curves in Fig. 7.

Equation (5) performs an integration over the Auger electron energies, eliminating the characteristic line-shape features of ARRE. The reduced intensity under detuned excitation is therefore a more general phenomenon and is not related only to ARRE. The curves in Fig. 7 can be considered as a special case of a widely employed electron yield measurement, which with a suitably selected electron energy range is known to represent well the absorption spectrum. Here we are, however, able to separate the features assigned to a specific resonance from the other features in the electron spectrum before determining the intensity curve (Fig. 7).

VII. CONCLUSIONS

The provided examples have demonstrated that the way ARRE is revealed in resonant Auger spectra and the strength of the effect depend largely on the conditions of the resonant excitation. The features that are often considered to be typical to ARRE, such as the linear dispersion of the Auger lines with the photon energy and the line shape, mimicking the shape of the photon band, are valid only as a special case of a narrow photon band. In a wide range of experimental situations, where the photon band is comparable with the lifetime width of the resonant state, the electron spectra display some quite specific features. The quantitative analysis of such spectra needs these features to be recognized and taken into account in the course of data handling. Several effects such as the tail cutoff, asymmetrical line shapes (or even peak doubling), and nonlinear energy dispersion may easily lead to untrue interpretations if the traditional data handling techniques (e.g., curve fitting with Voigt profiles) are applied.

The spectra recorded with a detuned photon band could be inevitable when studying close-lying resonance states. Such spectra may even be produced accidentally with slightly wrong tuning of the monochromator. It is essential to recognize the effects caused by the detuning and to not assign them any physical cause other than being purely a result of the interplay with the measurement device. ARRE may also occur together with the lifetime interference effect, in which case a successful interpretation of the experimental results may require both effects to be taken into account.

ACKNOWLEDGMENTS

We are grateful to Dr. Ergo Nõmmiste and the staff of MAX-laboratory for assistance and cooperation during the measurements. Financial support from the Research Council for Natural Sciences of the Academy of Finland is acknowledged.

[1] G.S. Brown, M.H. Chen, B. Crasemann, and G.E. Ice, Phys. Rev. Lett. **45**, 1937 (1980).
[2] G.B. Armen, T. Åberg, J.C. Levin, B. Crasemann, M.H. Chen, G.E. Ice, and G.S. Brown, Phys. Rev. Lett. **54**, 1142 (1985).
[3] A. Kivimäki, A. Naves de Brito, S. Aksela, H. Aksela, O.-P. Sairanen, A. Ausmees, S.J. Osborne, L.B. Dantas, and S. Svensson, Phys. Rev. Lett. **71**, 4307 (1993).
[4] Z.F. Liu, G.M. Bancroft, K.H. Tan, and M. Schachter, Phys. Rev. Lett. **72**, 621 (1994).
[5] H. Aksela, S. Aksela, O.-P. Sairanen, A. Naves de Brito, E. Nõmmiste, J. Tulkki, S. Svensson, A. Ausmees, and S.J. Osborne, Phys. Rev. A **49**, R4269 (1994).
[6] F. Gel'mukhanov and H. Ågren, Phys. Rev. A **49**, 4378 (1994).
[7] F. Gel'mukhanov and H. Ågren, Phys. Lett. A **193**, 375 (1994).
[8] T. Åberg, Phys. Scr. **T41**, 71 (1992).
[9] T. Åberg and B. Crasemann, in *X-Ray Resonant Anomalous Scattering*, edited by K. Fischer, G. Materlik, and C. Sparks (Elsevier, Amsterdam, 1994).
[10] G. Armen and H. Wang, Phys. Rev. A **51**, 1241 (1995).
[11] S. Aksela, E. Kukk, H. Aksela, and S. Svensson, Phys. Rev. Lett. **74**, 2917 (1995).
[12] N. Correira, A. Flores-Riveros, H. Ågren, K. Helenelund, L. Asplund, and U. Gelius, J. Chem. Phys. **83**, 2035 (1985).
[13] A. Cesar and H. Ågren, Phys. Rev. A **45**, 2833 (1992).
[14] S. J. Osborne, A. Ausmees, S. Svensson, A. Kivimäki, O.-P. Sairanen, A. Naves de Brito, H. Aksela, and S. Aksela, J. Chem. Phys. **102**, 7317 (1995).
[15] S. Aksela, A. Kivimäki, A. Naves de Brito, O.-P. Sairanen, S. Svensson, and J. Väyrynen, Rev. Sci. Instrum. **65**, 831 (1994).
[16] S. Aksela, A. Kivimäki, O.-P. Sairanen, A. Naves de Brito, E. Nõmmiste, and S. Svensson, Rev. Sci. Instrum. **66**, 1621 (1995).
[17] S. Aksela, A. Kivimäki, R. Nyholm, and S. Svensson, Rev. Sci. Instrum. **63**, 1252 (1992).
[18] S.J. Osborne, A. Ausmees, J.O Forsell, B. Wannberg, G. Bray, L.B. Dantas, S. Svensson, A. Naves de Brito, A. Kivimäki, and S. Aksela, Synchtrotron Radiat. News **7(1)**, 25 (1994).
[19] H. Aksela, J. Jauhiainen, E. Kukk, E. Nõmmiste, S. Aksela, and J. Tulkki, Phys. Rev. A **53**, 290 (1996).